

## Computation of eigenmodes on a compact hyperbolic space

KAIKI TARO INOUE

*Yukawa Institute for Theoretical Physics  
Kyoto University, Kyoto 606-8502, Japan*

### ABSTRACT

Measurements of CMB anisotropy are ideal experiments for discovering the non-trivial global topology of the universe. To evaluate the CMB anisotropy in multiply-connected(MC) compact cosmological models, one needs to compute the eigenmodes of the Laplace-Beltrami operator. We numerically obtain the low-lying eigenmodes on a compact 3-hyperbolic space called  $m003(-2, 3)$  in the SnapPea using the direct boundary element method. The computed eigenmodes are expanded in terms of eigenmodes on the unit three-dimensional pseudosphere. We numerically find that the expansion coefficients behave as gaussian pseudo-random numbers for low-lying eigenmodes.

# 1 Introduction

In recent years, there has been a great interest in properties of CMB anisotropy in multiply-connected (MC) cosmological models [1, 2, 3, 4]. Most of these studies deal with flat models or non-compact hyperbolic models for which the eigenmodes are known explicitly. Note that the eigenmodes are essential for analyzing the properties of CMB anisotropy. Since no closed analytic expression of the eigenmodes is known for compact hyperbolic (CH) models, so far, analysis of the CMB anisotropy in CH models has been considered to be quite difficult.

Computing the eigenmodes of the Laplace-Beltrami operator acting on a CH space (manifold) is equivalent to solving the Helmholtz equation with appropriate periodic boundary conditions in the universal covering space. A number of numerical methods have been used for solving the Helmholtz equation such as the finite element methods and the finite difference methods. In these methods, eigenfunctions are approximated by low-order polynomials and the integral representation of the Helmholtz equation is rewritten as the generalized eigenvalue problem. Therefore, one can obtain eigenvalues at once. These methods rely on the variational principle and yield upper bounds for the eigenvalues.

A numerical method called the "direct boundary element method" (DBEM) is used by Aurich and Steiner for finding out the eigenmodes of the Laplace operator on a two-dimensional compact MC space [5]. We find that this pioneering work is very useful not only for "quantum chaology", the study of the imprints of classical chaos in the quantum mechanical counterparts but also for the study of the CMB anisotropy in CH cosmological models. The advantage of the DBEM is that it enables one to compute the eigenfunctions much precisely than other methods as it does not rely on the variational principle and it uses an analytical fundamental solution, namely free Green's function. Since one needs to discretize only the boundary, generation of meshes is much easier than the other methods. Furthermore, as we shall see later, the DBEM is suitable for expanding the eigenfunctions that are continued onto the whole Poincaré ball by the periodic boundary conditions in terms of eigenfunctions on the pseudosphere<sup>1</sup>. Because the eigenfunction

---

<sup>1</sup>A set of the continued eigenfunctions is a subset of all eigenfunctions on the universal covering space.

at an arbitrary point either inside or outside the fundamental domain can be computed by using the values of the eigenfunction and their normal derivatives on the boundary.

In this paper, we introduce the DBEM for solving the Helmholtz equation, and describe the basic aspects of three-dimensional hyperbolic spaces. Then we apply the DBEM for computing the low-lying eigenmodes of the Laplace-Beltrami operator acting on a three-dimensional CH space(manifold)  $m003(-2,3)$ . The computed eigenfunctions are naturally continued onto the whole Poincaré ball because of the periodic boundary conditions and are expanded in terms of eigenmodes on the simply-connected pseudosphere. Statistical properties of the expansion coefficients are examined, since they are key factors in understanding of the CMB anisotropy in CH models.

## 2 The direct boundary element method (DBEM)

The boundary element methods (BEM) use free Green's function as the weighted function, and the Helmholtz equation is rewritten as an integral equation defined on the boundary using Green's theorem. Discretization of the boundary integral equation yields a system of linear equations. To locate an eigenvalue, the DBEM<sup>2</sup> requires one to compute many determinants of the corresponding boundary matrices which are dependent on the wavenumber  $k$ . Compared with other numerical methods such as the finite element method, the computing time for finding out the eigenmodes is much longer.

Firstly, let us consider the Helmholtz equation

$$(\nabla^2 + k^2)u(\mathbf{x}) = 0, \quad (1)$$

which is defined on a compact  $M$ -dimensional connected and simply-connected domain  $\Omega$  which is a subspace of a  $M$ -dimensional Riemannian manifold  $\mathcal{M}$ , with certain boundary conditions.  $\nabla^2 \equiv \nabla^i \nabla_i$ , ( $i = 1, 2, \dots, M$ ), and  $\nabla_i$  is the covariant derivative operator defined on  $\mathcal{M}$ . A square-integrable function  $u$  is the solution

---

<sup>2</sup>The DBEM uses only boundary points in evaluating the integrand in Eq.(5). The indirect methods use internal points in evaluating the integrand in Eq.(5) as well as the boundary points.

of the Helmholtz equation if and only if

$$\mathcal{R}[\bar{u}(\mathbf{x}), v(\mathbf{x})] \equiv \left\langle (\nabla^2 + k^2) u(\mathbf{x}), v(\mathbf{x}) \right\rangle = 0, \quad (2)$$

where  $v$  is an arbitrary square-integrable function called *weighted function* and  $\langle \rangle$  is defined as

$$\langle a, b \rangle \equiv \int_{\Omega} ab \, dV. \quad (3)$$

Next, we put  $u(\mathbf{x})$  into the form

$$u = \sum_{j=1}^M u_j \phi_j, \quad (4)$$

where  $\phi_j$ 's are linearly independent square-integrable functions. Numerical methods such as the finite element methods try to minimize the residue function  $\mathcal{R}$  for a fixed weighted function  $v(\mathbf{x})$  by changing the coefficients  $u_j$ . In these methods, one must resort to the variational principle to find the  $u_j$ 's which minimize  $\mathcal{R}$ .

Now we formulate the DBEM which is a version of BEMs. First, we slightly modify Eq.(2) using the Green's theorem

$$\int_{\Omega} (\nabla^2 u) v \sqrt{g} dV - \int_{\Omega} (\nabla^2 v) u \sqrt{g} dV = \int_{\partial\Omega} (\nabla_i u) v \sqrt{g} dS^i - \int_{\partial\Omega} (\nabla_i v) u \sqrt{g} dS^i, \quad (5)$$

where  $g \equiv \det\{g_{ij}\}$  and  $dV \equiv dx_1 \dots dx_M$ ; the surface element  $dS^i$  is given by

$$dS_i \equiv \frac{1}{M!} \epsilon_{ij_1 \dots j_M} dS^{j_1 \dots j_M},$$

$$dS^{j_1 \dots j_M} \equiv \begin{vmatrix} dx^{(1)j_1} & dx^{(2)j_1} & \dots & dx^{(M)j_1} \\ dx^{(1)j_2} & dx^{(2)j_2} & \dots & dx^{(M)j_2} \\ \vdots & \vdots & \ddots & \vdots \\ dx^{(1)j_M} & dx^{(2)j_M} & \dots & dx^{(M)j_M} \end{vmatrix}, \quad (6)$$

where  $\epsilon_{j_1 \dots j_{M+1}}$  denotes the  $M+1$ -dimensional Levi-Civita tensor. Then Eq.(2) becomes

$$\int_{\Omega} (\nabla^2 v + k^2 v) u \sqrt{g} dV + \int_{\partial\Omega} (\nabla_i u) v \sqrt{g} dS^i - \int_{\partial\Omega} (\nabla_i v) u \sqrt{g} dS^i = 0. \quad (7)$$

As the weighted function  $v$ , we choose the fundamental solution  $G_E(\mathbf{x}, \mathbf{y})$  which satisfies

$$(\nabla^2 + E)G_E(\mathbf{x}, \mathbf{y}) = \delta_D(\mathbf{x} - \mathbf{y}), \quad (8)$$

where  $E \equiv k^2$ , and  $\delta_D(\mathbf{x} - \mathbf{y})$  is Dirac's delta function.  $G_E(\mathbf{x}, \mathbf{y})$  is also known as the free Green's function defined on  $\mathcal{M}$ . Let  $\mathbf{y}$  be an internal point of  $\Omega$ . Then we obtain from Eq.(7) and Eq.(8),

$$u(\mathbf{y}) + \int_{\partial\Omega} G_E(\mathbf{x}, \mathbf{y}) \nabla_i u \sqrt{g} dS^i - \int_{\partial\Omega} (\nabla_i G_E(\mathbf{x}, \mathbf{y})) u \sqrt{g} dS^i = 0. \quad (9)$$

Thus the values of eigenfunctions at internal points can be computed using only the boundary integral. If  $\mathbf{y} \in \partial\Omega$ , we have to evaluate the limit of the boundary integral terms as  $G_E(\mathbf{x}, \mathbf{y})$  becomes divergent at  $\mathbf{x} = \mathbf{y}$  [6]. The boundary integral equation is finally written as

$$\frac{1}{2}u(\mathbf{y}) + \int_{\partial\Omega} G_E(\mathbf{x}, \mathbf{y}) \nabla_i u \sqrt{g} dS^i - \int_{\partial\Omega} (\nabla_i G_E(\mathbf{x}, \mathbf{y})) u \sqrt{g} dS^i = 0, \quad (10)$$

or in another form,

$$\frac{1}{2}u(\mathbf{y}) + \int_{\partial\Omega} G_E(\mathbf{x}, \mathbf{y}) \frac{\partial u}{\partial x^i} n^i \sqrt{g} dS - \int_{\partial\Omega} \frac{\partial G_E(\mathbf{x}, \mathbf{y})}{\partial x^i} n^i u \sqrt{g} dS = 0, \quad (11)$$

where  $n^i \equiv dS^i/dS$  and  $dS \equiv \sqrt{dS^i dS_i}$ . Note that we assumed that the boundary surface at  $\mathbf{y}$  is sufficiently smooth <sup>3</sup>. We see from Eq.(10) or Eq.(11) that the approximated solutions can be obtained without resorting to the variational principle. Since it is virtually impossible to solve Eq.(11) analytically, we discretize it using boundary elements. Let the number of the elements be  $N$ . We approximate  $u$  by some low-order polynomials (shape function), *e.g.*  $u = c_1 + c_2 \eta + c_3 \xi$ . Then we have the following equation:

$$[H]\{u\} = [G]\{q\}, \quad q \equiv \frac{\partial u}{\partial n}, \quad (12)$$

where  $\{u\}$  and  $\{q\}$  are  $N$ -dimensional vectors which consist of the boundary values of an eigenfunction and its normal derivatives, respectively.  $[H]$  and  $[G]$  are  $N \times N$ -dimensional coefficient matrices which are obtained from integration of the fundamental solution  $G_E(\mathbf{x}, \mathbf{y})$  and its normal derivatives multiplied by  $u_i$  and  $q_i$ , respectively. The explicit form of  $[H]$  and  $[G]$  for constant elements are given in section 4. Note that elements in  $[H]$  and  $[G]$  include  $k$  implicitly. Because Eq.(12)

---

<sup>3</sup>If  $y$  is located at a corner on the boundary, one must carefully evaluate Eq.(9). A convenient way is to rewrite Eq.(9) in a regularized form [7].

includes both  $u$  and  $q$ , the boundary element method can naturally incorporate the periodic boundary conditions:

$$u(\mathbf{x}) = u(g(\mathbf{x})), \quad q(\mathbf{x}) = -q(g(\mathbf{x})), \quad \text{on } \partial\Omega, \quad g \in \Gamma, \quad (13)$$

where  $\Gamma$  denotes a discrete isometry group. The boundary conditions constrain the number of unknown constants to  $N$ . Application of the boundary condition (13) to Eq.(12) and permutation of the columns of the components yields

$$[A]\{x\} = 0, \quad (14)$$

where  $N \times N$ -dimensional matrix  $A$  is constructed from  $G_{ij}$  and  $H_{ij}$  and  $N$ -dimensional vector  $x$  is constructed from  $u_i$ 's and  $q_i$ 's. For the presence of the non-trivial solution, the following relation must hold,

$$\det[A] = 0. \quad (15)$$

Thus the eigenvalues of the Laplace-Beltrami operator acting on a compact space are obtained by searching for  $k$ 's which satisfy Eq.(15).

### 3 Three-dimensional hyperbolic spaces

The discrete subgroup  $\Gamma$  of  $PSL(2, \mathbb{C})$  which is the orientation-preserving isometry group of the simply-connected 3-hyperbolic space  $\mathbb{H}^3$  is called the Kleinian group. Any CH space (either manifold or orbifold) can be described as compact quotients  $\mathcal{M} = \mathbb{H}^3/\Gamma$ . The classification of the Kleinian group is not completed. However, several procedures for constructing compact hyperbolic spaces are known. Before going into detail, we present some elements of the three-dimensional hyperbolic geometry.

The standard pseudospherical coordinates  $(\chi, \theta, \phi)$  for  $\mathbb{H}^3$  with curvature radius  $R$  are given by

$$\begin{aligned} X_0 &= R \cosh \chi, & X_1 &= R \sinh \chi \sin \theta \cos \phi \\ X_2 &= R \sinh \chi \sin \theta \sin \phi, & X_3 &= R \sinh \chi \cos \theta \end{aligned} \quad (16)$$

with

$$0 \leq \chi < \infty, \quad 0 \leq \theta < \pi, \quad 0 \leq \phi < 2\pi. \quad (17)$$

In these coordinates, the line element takes the form

$$ds^2 = \sum_{i=0}^3 (dX_i)^2 = R^2 [d\chi^2 + \sinh \chi^2 (d\theta^2 + \sin^2 \theta d\phi^2)]. \quad (18)$$

The Poincaré representation is obtained by the transformation

$$x_1 = R \tanh \frac{\chi}{2} \sin \theta \cos \phi, \quad x_2 = R \tanh \frac{\chi}{2} \sin \theta \sin \phi, \quad x_3 = R \tanh \frac{\chi}{2} \cos \theta, \quad (19)$$

which maps  $\mathbb{H}^3$  into the open ball  $\{(x_1, x_2, x_3) \in \mathbb{E}^3 \mid x_1^2 + x_2^2 + x_3^2 < R^2\}$  called the *Poincaré ball*. The line element in these coordinates takes the form

$$ds^2 = \frac{4(dx_1^2 + dx_2^2 + dx_3^2)}{\left(1 - \frac{x_1^2 + x_2^2 + x_3^2}{R^2}\right)^2}, \quad (20)$$

and the geodesic distance  $d$  between  $\mathbf{x}$  and  $\mathbf{x}'$  is given by

$$\cosh[R^{-1}d(\mathbf{x}, \mathbf{x}')] = 1 + \frac{2|\tilde{\mathbf{x}} - \tilde{\mathbf{x}}'|^2}{(1 - |\tilde{\mathbf{x}}|^2)(1 - |\tilde{\mathbf{x}}'|^2)}. \quad (21)$$

where  $\tilde{\mathbf{x}} = R^{-1}\mathbf{x}$ ,  $\tilde{\mathbf{x}}' = R^{-1}\mathbf{x}'$ . Note that geodesics in the Poincaré ball are either diameters or semi-circles which orthogonally intersect with the boundary of the Poincaré ball.

Another commonly used set of coordinates is obtained from the upper-half space representation which is defined by the transformation

$$\begin{aligned} y_1 &= \frac{\sinh \chi \sin \theta \cos \phi}{D}, \quad y_2 = \frac{\sinh \chi \sin \theta \sin \phi}{D}, \quad y_3 = \frac{1}{D}, \\ D &= \cosh \chi - \sinh \chi \cos \theta, \end{aligned} \quad (22)$$

which maps  $\mathbb{H}^3$  into the upper-half space  $\mathbb{E}_+^3 = \{(y_1, y_2, y_3) \in \mathbb{E}^3 \mid y_3 > 0\}$ . In these coordinates, the line element takes the form

$$ds^2 = \frac{R^2(dy_1^2 + dy_2^2 + dy_3^2)}{y_3^2}. \quad (23)$$

The geodesic distance is given by

$$\cosh[R^{-1}d(\mathbf{y}, \mathbf{y}')] = 1 + \frac{|\mathbf{y} - \mathbf{y}'|^2}{2y_3y'_3}. \quad (24)$$

In the upper-half space model, geodesics are either straight vertical lines or semi-circles orthogonal to the boundary of the upper-half space. The orientation-preserving isometry of  $\mathbb{H}^3$ ,  $PSL(2, \mathbb{C})$  induces a transformation  $\gamma$  on the boundary of the complex plane( $y_1, iy_2$ ):

$$\gamma : z \rightarrow z' = \frac{az + b}{cz + d}, \quad ad - bc = 1, \quad z \equiv y_1 + iy_2, \quad (25)$$

where a, b, c and d are complex numbers. The transformation  $\gamma$  on the complex plane( $y_1, iy_2$ ) can be uniquely lifted onto  $\mathbb{H}^3$  as an orientation-preserving isometry [8],

$$\begin{aligned} \tilde{\gamma} : \mathbb{H}^3 \cup \mathbb{C} \cup \{\infty\} &\rightarrow \mathbb{H}^3 \cup \mathbb{C} \cup \{\infty\}, \\ \tilde{\gamma} : (z(y_1, y_2), y_3) &\rightarrow \left( \frac{(az + b)(\overline{cz + d}) + a\bar{c}y_3^2}{|cz + d|^2 + |c|^2y_3^2}, \frac{y_3}{|cz + d|^2 + |c|^2y_3^2} \right). \end{aligned} \quad (26)$$

$\gamma$  is called the *Möbius transformation*, and  $\tilde{\gamma}$  is called the *extended Möbius transformation*.

In the *Klein* (projective) model, the geodesics and planes are mapped into their Euclidean counterparts. Since the fundamental domain is enclosed by Euclidean planes in the Klein coordinates, the task of generating meshes is much easier than other coordinates. The transformation

$$z_1 = R \tanh \chi \sin \theta \cos \phi, \quad z_2 = R \tanh \chi \sin \theta \sin \phi, \quad z_3 = R \tanh \chi \cos \theta \quad (27)$$

can be understood as the projection of the hyperboloid  $(X_0, X_1, X_2, X_3)$  onto the interior of the sphere  $(R, z_1, z_2, z_3)$  along lines originating from the origin (0,0,0,0). The geodesic distance can be represented as

$$\cosh[R^{-1}d(\mathbf{z}, \mathbf{z}')] = \frac{1 - \tilde{\mathbf{z}} \cdot \tilde{\mathbf{z}'}}{\sqrt{(1 - |\tilde{\mathbf{z}}|^2)(1 - |\tilde{\mathbf{z}}'|^2)}}. \quad (28)$$

where  $\tilde{\mathbf{z}} = R^{-1}\mathbf{z}$ ,  $\tilde{\mathbf{z}}' = R^{-1}\mathbf{z}'$ .



Until late 1970's, only several CH manifolds were known. In 1931, Löbell constructed a CH manifold whose fundamental domain is a polyhedron with 14 faces, two faces being regular hexagons and the twelve faces being regular pentagons [9]. In 1933, Seifert and Weber found a CH manifold whose fundamental domain is a regular dodecahedron [10]. In 1971, Best showed that an icosahedron can also be the fundamental domain. There are three ways in gluing the faces [11].

In late 1970's, Thurston found an algorithm to make an infinite number of sequences of CH manifolds which are topologically inequivalent [12, 13]. Suppose a knot or a link  $X$  in  $\widehat{\mathbb{E}^3} \equiv \mathbb{E}^3 + \{\infty\}$  or equivalently  $\mathbb{S}^3$ . If  $X$  is "appropriate", the compliment space of  $X$  is homeomorphic to a certain non-compact hyperbolic manifold. To make a sequence of compact manifolds, one needs to remove the tubular neighborhood of  $X$ , whose boundary is homeomorphic to a torus and it is glued back with another solid torus by a twisted map represented by a pair of integer  $(p, q)$  so that closed curves  $pa + qb = 0$  on the boundary of the solid torus can shrink to points by continuous deformation. This procedure is called Dehn's surgery. By this method, one obtains a countably infinite number of topologically inequivalent manifolds that admit a hyperbolic structure except for a finite number of pairs. It is known that all the CH manifolds can be obtained by Dehn's surgery [13]. Description of a class of  $X$  that yields CH manifolds is the remaining task for the complete understanding of the classification of CH manifolds.

There is an essential difference between two-dimensional cases and higher dimensional cases. According to Mostow's rigidity theorem, if two CH manifolds, with dimension higher than two, have isomorphic fundamental groups, they are necessarily isometric each other whereas in the two-dimensional case, there are an infinite number of hyperbolic manifolds which have the same fundamental group [14]. It is known that there are only finitely many different three-dimensional CH manifolds with the same volume [15]. Thus the volume of a CH manifold is an "almost-invariant" quantity which classifies CH manifolds.

The possible values for the volume of the CH manifolds are bounded below and no upper bound exists. The minimal value has not yet been known, although Meyerhoff has proved that  $Vol_{\min} > 0.00082R^3$ . Thurston proposed a manifold  $Q_2$  as a candidate for the three-dimensional hyperbolic manifold of the

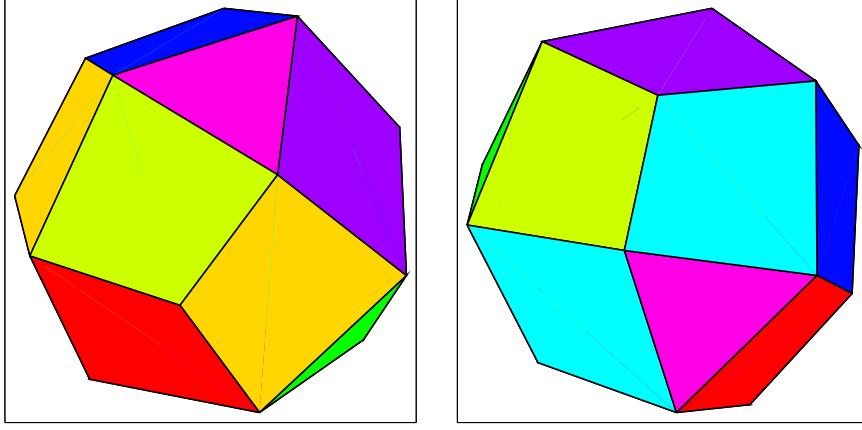


Figure 1: Fundamental domain of m003(-2,3)

minimum volume  $Vol(Q_2) = 0.98139R^3$  [16]. However, Weeks [17] and independently, Matveev and Fomenko [18] discovered a CH manifold  $Q_1$  with the smallest value  $Vol(Q_1) = 0.94272R^3$  in the known CH manifolds and it is conjectured to be the one with the minimum volume. A computer program "SnapPea" by Jeff Weeks [19] has made it possible to catalog and study a large number of CH and non-CH spaces which include  $Q_1, Q_2$  and thousands of cusped and non-cusped hyperbolic 3-manifolds.

Let us see how CH manifolds are characterized in the SnapPea. Any element of the discrete isometry group  $\Gamma$  which is equivalent to the fundamental group  $\pi_1(\mathcal{M})$  can be described as a *word* which is a product of generators  $\{g_1, \dots, g_s\}$ ,

$$g = \prod_j g_{m_j}^{n_j}, \quad (j, n_j \in \mathbb{Z}, \quad m_j = 1, \dots, s), \quad g \in \Gamma. \quad (29)$$

The above expression is not unique, since they are subject to a set of relations, each of which takes the form,

$$\mathcal{I} = \prod_j g_{l_j}^{k_j} \quad (j, k_j \in \mathbb{Z}, \quad l_j = 1, \dots, s). \quad (30)$$

Note that different expression of  $g$  is possible by choosing different generators. In the case of Thurston's manifold  $Q_2$  which is cataloged as m003(-2,3) in the SnapPea,  $\Gamma$  has a simple presentation,

$$\Gamma = \{a, b : ab^3aba^{-2}b, \quad ab^{-1}a^{-1}baba^{-1}b^{-1}ab^{-1}\}, \quad (31)$$

where  $a$  and  $b$  are generators and words in the parenthesis are equal to identities. This representation is simple for describing  $\Gamma$  but not convenient for describing the fundamental domain. Choosing a coordinate system centered at a point of locally maximum of the injectivity radius<sup>4</sup>, generators which define the face identification maps can be represented by eight matrices (see SnapPea), which imply that the number of the faces on the boundary of the fundamental domain is sixteen. The face identifications are shown in Fig.1, in which each color of the faces corresponds to one of the identification maps. The figures on the left side and the right side show the fundamental domain which is viewed from a point  $(0,0,-1000)$  and from a point  $(0,0,1000)$  in the Klein coordinates, respectively.

---

<sup>4</sup>The injectivity radius of a point  $p$  is equal to half the length of the shortest periodic geodesic on  $p$ .

## 4 Computation of low-lying eigenmodes

In this section, we apply the DBEM for computing the low-lying eigenmodes on a CH space called m003(-2,3).

The Helmholtz equation in the Poincaré coordinates is written as

$$\frac{1}{4} \left( 1 - \frac{2}{1 - |\mathbf{x}|^2} \right)^2 \left[ \Delta_E + \frac{2}{1 - |\mathbf{x}|^2} \mathbf{x} \cdot \nabla_E \right] u + k^2 u = 0, \quad (32)$$

where  $\Delta_E$  and  $\nabla_E$  are the Laplacian and the gradient on the corresponding three-dimensional Euclidean space, respectively. Note that we have set the curvature radius  $R = 1$  without loss of generality. By using the DBEM, the Helmholtz equation (32) is converted to an integral representation on the boundary. Here Eq.(11) can be written in terms of Euclidean quantities as

$$\frac{1}{2} u(\mathbf{y}) + \int_{\partial\Omega} G_k(\mathbf{x}, \mathbf{y}) \frac{\partial u}{\partial x^i} n_E^i dS - \int_{\partial\Omega} \frac{\partial G_k(\mathbf{x}, \mathbf{y})}{\partial x^i} u n_E^i dS = 0, \quad (33)$$

where  $dS = 2(1 - |\mathbf{x}|^2)^{-1} dS_E$ . The fundamental solution is given as [20, 21]

$$G_k(\mathbf{x}, \mathbf{y}) = -\frac{1}{4\pi} \frac{(\sigma + \sqrt{\sigma^2 - 1})^{-s}}{\sqrt{\sigma^2 - 1}}, \quad -\frac{\pi}{2} < \arg s \leq \frac{\pi}{2}, \quad (34)$$

where  $s = \sqrt{1 - k^2}$  and  $\sigma = \cosh d(\mathbf{x}, \mathbf{y})$ . Then Eq.(33) is discretized on the boundary elements  $\Gamma_J$  as

$$\frac{1}{2} u(\mathbf{x}_I) + \sum_{J=1}^N \left[ \int_{\Gamma_J} G_k(\mathbf{x}_I, \mathbf{y}_J) \frac{\partial u(\mathbf{y}_J)}{\partial n} dS - \int_{\Gamma_J} \frac{\partial G_k(\mathbf{x}_I, \mathbf{y}_J)}{\partial n} u(\mathbf{y}_J) dS \right] = 0, \quad (35)$$

where  $N$  denotes the number of the boundary elements. An example of  $N = 1168$  elements on the boundary of the fundamental domain in the Poincaré coordinates is shown in Fig.2. The maximum length of the edge  $\Delta l$  in these elements is 0.14. The condition that the corresponding de Broglie wavelength  $2\pi/k$  is longer than the four times of the interval of the boundary elements yields a rough estimate of the validity condition of the calculation as  $k < 11$ . On each  $\Gamma_J$ ,  $u$  and  $q \equiv \partial u / \partial n$  are approximated by low order polynomials. For simplicity, we use constant elements:

$$u(\mathbf{x}_J) = u^J = \text{Const.}, \quad q(\mathbf{x}_J) = q^J = \text{Const.}, \quad \text{on } \Gamma_J. \quad (36)$$

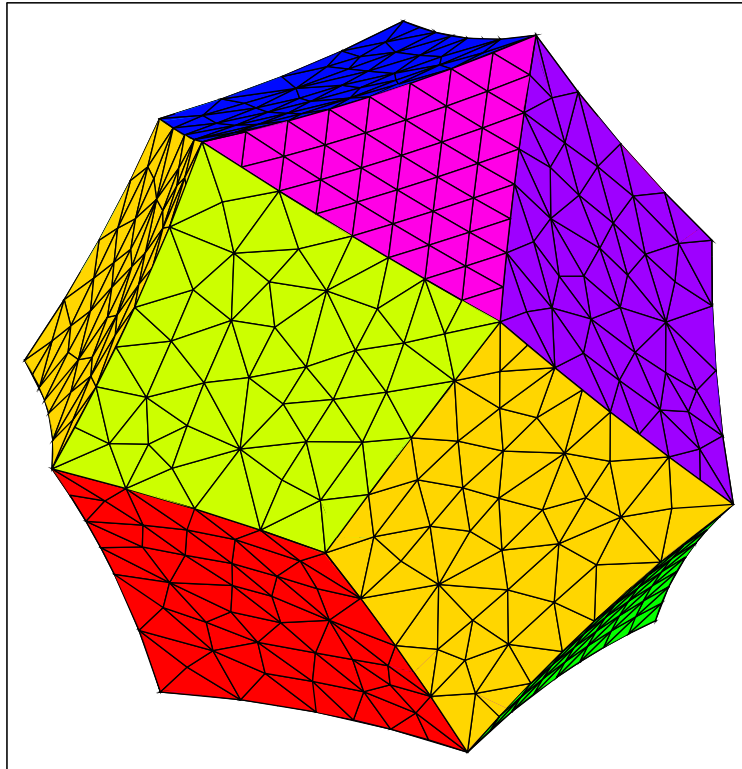


Figure 2: 1168 boundary elements

Substituting Eq.(36) into Eq.(35), we obtain

$$\sum_{J=1}^N H_{IJ} u^J = \sum_{J=1}^N G_{IJ} q^J,$$

$$H_{IJ} = \begin{cases} \tilde{H}_{IJ} & I \neq J \\ \tilde{H}_{IJ} - \frac{1}{2} & I = J, \end{cases}$$

where

$$\tilde{H}_{IJ} \equiv \int_{\Gamma_J} \frac{\partial G_k}{\partial n}(\mathbf{x}_I, \mathbf{y}_J) dS(\mathbf{y}_J), \quad G_{IJ} \equiv \int_{\Gamma_J} G_k(\mathbf{x}_I, \mathbf{y}_J) dS(\mathbf{y}_J). \quad (37)$$

The singular integration must be carried out for I-I components as the fundamental solution diverges at  $(\mathbf{x}_I = \mathbf{y}_I)$ . This is not an intractable problem. Several numerical techniques have already been proposed by some authors [22, 23]. We have applied Hayami's method to the evaluation of the singular integrals [23]. Introducing coordinates similar to spherical coordinates centered at  $\mathbf{x}_I$ , the singularity is canceled out by the Jacobian which makes the integral regular.

Let  $g_i$  ( $i=1, 2, \dots, 8$ ) be the generators of the discrete group  $\Gamma$  which identify a boundary face  $F_i$  with another boundary face  $g_i(F_i)$ :

$$g_i(\mathbf{x}_i) = \mathbf{x}_i, \quad \mathbf{x}_i \in F_i. \quad (38)$$

The boundary of the fundamental domain can be divided into two regions  $\partial\Omega_A$  and  $\partial\Omega_B$  and each of them consists of  $N/2$  boundary elements,

$$\partial\Omega_A = \cup F_i, \quad \partial\Omega_B = \cup g_i(F_i), \quad i = 1, 2, \dots, 8. \quad (39)$$

The periodic boundary conditions

$$u(g_i(\mathbf{x}_i)) = u(\mathbf{x}_i), \quad q(g_i(\mathbf{x}_i)) = -q(\mathbf{x}_i), \quad i = 1, 2, \dots, 8 \quad (40)$$

reduce the number of the independent variables to  $N$ , *i.e.* for all  $\mathbf{x}_B \in \partial\Omega_B$ , there exist  $g_i \in \Gamma$  and  $\mathbf{x}_A \in \partial\Omega_A$  such that

$$u(\mathbf{x}_B) = u(g_i(\mathbf{x}_A)) = u(\mathbf{x}_A), \quad q(\mathbf{x}_B) = -q(g_i(\mathbf{x}_A)) = -q(\mathbf{x}_A). \quad (41)$$

Substituting the above relation into Eq.(37), we obtain

$$\begin{bmatrix} H_{AA} + H_{AB} & -G_{AA} + G_{AB} \\ H_{BA} + H_{BB} & -G_{BA} + G_{BB} \end{bmatrix} \begin{Bmatrix} u_A \\ q_A \end{Bmatrix} = 0, \quad (42)$$

k	$m_k$
5.41	1
5.79	1
6.81	1
6.89	1
7.12	1
7.69	1
8.30	1
8.60	1
8.73	1
9.26	2
9.76	1
9.91	1
9.99	1

Table 1: Eigenvalue  $k$  and multiplicity  $m_k$

where  $u_A = (u^1, u^2, \dots, u^{N/2})$  and  $q_A = (q^1, q^2, \dots, q^{N/2})$  and matrices  $H = \{H_{IJ}\}$  and  $G = \{G_{IJ}\}$  are written as

$$H = \begin{bmatrix} H_{AA} & H_{AB} \\ H_{BA} & H_{BB} \end{bmatrix}, \quad G = \begin{bmatrix} G_{AA} & G_{AB} \\ G_{BA} & G_{BB} \end{bmatrix}. \quad (43)$$

Eq. (42) takes the form

$$[A(k)]\{x\} = 0, \quad (44)$$

where  $N \times N$ -dimensional matrix  $A$  is constructed from  $G$  and  $H$  and  $N$ -dimensional vector  $x$  is constructed from  $u_A$  and  $q_A$ . For the presence of the non-trivial solution, the following relation must hold,

$$\det[A(k)] = 0. \quad (45)$$

Thus the eigenvalues of the Laplace-Beltrami operator acting on a compact space are obtained by searching for  $k$ 's which satisfy Eq.(45). In practice, Eq.(45) cannot be exactly satisfied because of the numerical error. Instead, one must search for the local minima of  $\det[A(k)]$ . This process needs long computation time as  $A(k)$  depends on  $k$  implicitly. Our numerical result ( $k < 10$ ) is shown in Table 1.

The first "excited state" which corresponds to  $k = k_1$  is important for the

understanding of CMB anisotropy. Our numerical result  $k_1 = 5.41$  is consistent with the value 5.04 obtained from Weyl's asymptotic formula

$$N[\nu] = \frac{Vol(\mathcal{M})\nu^3}{6\pi^2}, \quad \nu \equiv \sqrt{k^2 - 1}, \quad \nu \gg 1, \quad (46)$$

assuming that no degeneracy occurs. One can interpret the first excited state as the mode that has the maximum de Broglie wavelength  $2\pi/k_1$ . Because of the periodic boundary conditions, the de Broglie wavelength can be approximated by the "average diameter" of the fundamental domain defined as a sum of the inradius  $r_-$  and the outradius  $r_+$ <sup>5</sup>, which yields  $k_1 = 4.9$  just 10% less than the numerical value. From these estimates, supercurvature modes in small CH spaces ( $Vol(\mathcal{M}) \sim 1$ ) are unlikely to be observed.

To compute the value of eigenfunctions inside the fundamental domain, one needs to solve Eq.(44). The singular decomposition method is the most suitable numerical method for solving any linear equation with a singular matrix  $A$ , which can be decomposed as

$$A = U^\dagger D V, \quad (47)$$

where  $U$  and  $V$  are unitary matrices and  $D$  is a diagonal matrix. If  $D_{ii}$  in  $D$  is almost zero then the complex conjugate of the  $i$ -th row in  $V$  is an approximated solution of Eq.(44). The number of the "almost zero" diagonal elements in  $D$  is equal to the multiplicity number. Substituting the values of the eigenfunctions and their normal derivatives on the boundary into Eq.(9), the values of the eigenfunctions inside the fundamental domain can be computed. Eigenfunctions  $k = 5.41$  and  $k = 9.99$  in Poincaré coordinates plotted as  $(x_1, x_2, h)$ , where  $h = u_\nu(x_1, x_2, 0.0087)$  are shown in Fig.3. The eigenfunctions we computed are all real-valued. Note that the non-degenerated eigenfunctions must be real-valued.

---

<sup>5</sup>The inradius  $r_-$  is the radius of the largest simply-connected sphere in the fundamental domain, and the outradius  $r_+$  is the radius of the smallest sphere that can enclose the fundamental domain.  $r_- = 0.535$ ,  $r_+ = 0.7485$  for m003(-2,3).



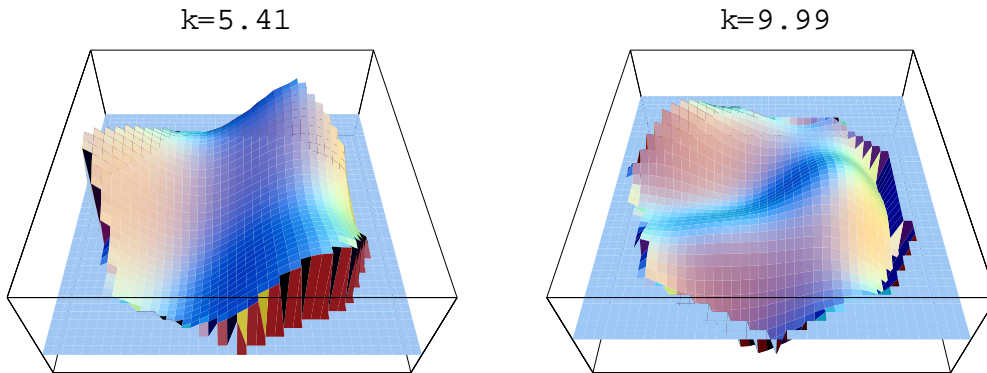


Figure 3: Eigenfunctions  $u_\nu$  on a slice  $x_3 = 0.0087$

## 5 Statistical properties of eigenmodes

Properties of eigenmodes of the Laplace-Beltrami operator are determined by the Helmholtz equation. Therefore, at first glance it does not seem to make a sense to study the statistical properties of the eigenmodes.

However, if one recognizes the Laplace-Beltrami operator acting on a CH space as the Hamiltonian in a quantum mechanical system, each eigenmode can be interpreted as a wavefunction in an eigenstate. Since the corresponding classical system is known to be a typical chaotic system (K-system), it is natural to assume that the imprints of classical chaos is hidden in the corresponding quantum system.

Recent studies have demonstrated that some of the statistical properties of energy spectrum are in accordance with the universal prediction of random-matrix theory(RMT) [24, 25]. RMT also predicts that the squared expansion coefficients  $|a_i|^2$  of an eigenstate with respect to a generic basis are gaussian distributed [27, 26, 5]. In the limit  $N \rightarrow \infty$ ,  $x = |a_i|^2$  obeys the statistics given for three universality classes of the orthogonal (GOE,  $\mu = 1$ ), unitary (GUE,  $\mu = 2$ ) and symplectic (GSE,  $\mu = 4$ ) ensembles, each distribution function  $P$  is given by

$$P_\mu(x) = \left(\frac{\mu}{2}\right)^{\mu/2} \Gamma(\mu/2) x^{\mu/2-1} e^{-\mu x/2}. \quad (48)$$

In our case, as the time-reversal symmetry of the Hamiltonian implies, one expects that  $|a_i|^2$  obeys the GOE prediction. In order to apply the GOE prediction to

the statistical properties of eigenstates on CH spaces, one needs to find a set of orthonormal basis but no closed analytic expression is known for any CH spaces. To avoid the problem, Aurich and Steiner noticed that the wavefunctions on the hyperbolic octagons can be continued onto the universal covering space  $\mathbb{H}^2$ , and eigenstates can be expanded in terms of circular-waves [5]. They numerically found that the squared expansion coefficients obeys the GOE prediction in highly excited states of a hyperbolic asymmetrical octagon model.

We extend their method to three-dimensional CH models where we consider only low-lying modes. First, we normalize the obtained 14 eigenfunctions on m003(-2,3). The eigenfunctions are naturally continued onto the whole unit Poincaré ball by the periodic boundary condition. As a "generic basis", we consider a set of orthonormal eigenfunctions  $Q_{\nu lm}$  (T-complete functions) on the unit pseudosphere which is isometric to the Poincaré ball,

$$\begin{aligned} Q_{\nu lm} &\equiv X_{\nu l}(\chi) Y_{lm}(\theta, \phi), \\ X_{\nu l} &\equiv (-1)^{l+1} \sqrt{\frac{2}{\pi}} \left( \prod_{n=0}^l (n^2 + \nu^2) \right)^{-1/2} \sinh^l \chi \frac{d^{l+1}(\cos \nu \chi)}{d(\cosh \chi)^{l+1}}, \\ &= \frac{\Gamma(l+1+\nu i)}{\Gamma(\nu i)} \sqrt{\frac{1}{\sinh \chi}} P_{\nu i-1/2}^{-l-1/2}(\cosh \chi), \quad \nu^2 = k^2 - 1, \end{aligned} \quad (49)$$

where  $P$ ,  $Y_{lm}$  and  $\Gamma$  denote the associated Legendre function, the spherical harmonics and gamma function, respectively.  $P$  can be written in terms of the hypergeometric function  ${}_2F_1$  [28],

$$P_{\nu i-1/2}^{-l-1/2}(\cosh \chi) = \frac{(\coth \frac{1}{2}\chi)^{-l-1/2}}{\Gamma(\frac{3}{2}+l)} {}_2F_1\left(\frac{1}{2}-\nu i, \frac{1}{2}+\nu i; \frac{3}{2}+l; -\sinh^2 \frac{1}{2}\chi\right). \quad (50)$$

Eigenfunctions  $u_\nu$  can be expanded in terms of  $Q_{\nu lm}$ 's as

$$u_\nu = \sum_{lm} \xi_{\nu lm} X_{\nu l}(\chi) Y_{lm}(\theta, \phi). \quad (51)$$

Note that each  $u_\nu$  has no components with  $\nu' \neq \nu$  because  $Q_{\nu lm}$ 's are complete and linearly independent.

At first glance the computation of  $\xi_{\nu lm}$  in Eq. (51) seems cumbersome as the

	$0 \leq l < 8$	$8 \leq l \leq 13$	$13 < l \leq 18$
$k < 8$	0.53	1.3	1.6
$k > 8$	0.53	1.1	1.3

Table 2: An example of choice of  $\chi_o$  for which the absolute value of  $X_{\nu l}(\chi_o)$  is not too small.

domain of the integration extends over the whole pseudosphere. Fortunately, one can obtain  $\xi_{\nu lm}$  by evaluating two-dimensional integrals.  $\xi_{\nu lm}$  can be written as

$$\xi_{\nu lm} X_{\nu l}(\chi_o) = \int u_{\nu}(\chi_o, \theta, \phi) Y_{lm}^*(\theta, \phi) d\Omega, \quad (52)$$

which is satisfied for the arbitrary value of  $\chi_o$ . In practice the numerical instability occurs in the region where the absolute value of  $X_{\nu l}$  is too small. In our computation, the values of  $\chi_o$  are chosen as shown in Table 2. Thus  $\xi_{\nu lm}$  can be computed if one obtains the values of eigenfunctions on the sphere

$$x_1 = \tanh \frac{\chi_o}{2} \sin \theta \cos \phi, \quad x_2 = \tanh \frac{\chi_o}{2} \sin \theta \sin \phi, \quad x_3 = \tanh \frac{\chi_o}{2} \cos \theta \quad (53)$$

with radius  $\chi_o$ .

In order to compute the values of eigenfunctions on the sphere with radius longer than the inradius  $r_- = 0.535$ , the points outside of the fundamental domain must be pulled back to the inside, since Eq.(9) is valid only if  $\mathbf{y}$  is a set of coordinates of an internal point.

The plots of eigenfunctions on a sphere  $\chi_o = 1.6$  are shown in Fig.4 and Fig.5. Apparent structure of the eigenfunctions on the sphere seems complicated. However, some regular patterns are hidden in the structure due to the periodic boundary conditions. Actually, there are pairs of highly correlated points on the sphere, since any partial surface  $S_{i1}$  of the sphere that is enclosed by copies of the boundary of the fundamental domain pulled back to inside the fundamental domain by the corresponding element of the discrete isometry group intersects another partial surface  $S_{i2}$  that is pulled back to inside the fundamental domain. To evaluate the correlation pattern, let us estimate how often a sphere with radius  $\chi = \chi_o$  intersects the copies of the fundamental domain. The approximate number  $n_1$  of the

copies of the fundamental domain inside the sphere with radius (in proper length)  $\chi_o$  is given by

$$n_1 = \frac{\pi(\sinh(2\chi_o) - 2\chi_o)}{Vol(Q_2)}. \quad (54)$$

From this formula, in the case of m003(-2,3),  $n_1 \sim 29$  if  $\chi_o = 1.6$ . Because the sphere intersects the fundamental domain at random, the copies of the fundamental domain on the sphere stick out their half portions on average. Therefore, the approximate number  $n_2$  of the copies that intersect the sphere is given by

$$n_2 = \frac{\pi(\sinh(2(\chi_o + r_{ave})) - \sinh(2(\chi_o - r_{ave})) - 4r_{ave})}{Vol(Q_2)}, \quad (55)$$

where  $r_{ave} = (r_+ + r_-)/2$ . This estimate gives  $n_2 \sim 120$  if  $\chi_o = 1.6$ . Approximating each eigenmode by de Broglie waves, we obtain the corresponding fluctuation scale  $\delta A$  in steradian on the sphere,

$$\begin{aligned} \delta A &= \frac{4\pi}{n_2} \frac{4\pi^2}{k^2} \\ &= \frac{16\pi^2 Vol(Q_2)}{k^2(\sinh(2(\chi_o + r_{ave})) - \sinh(2(\chi_o - r_{ave})) - 4r_{ave})}. \end{aligned} \quad (56)$$

Thus correlation patterns are observed in pairs of patches with typical size  $\delta A$ . When  $\chi_o = 1.6$ , angular fluctuation scales are given as  $\delta l \sim \sqrt{\delta A} = 21^\circ, 12^\circ$ , for  $k = 5.41, 9.99$ , respectively.

Next, we extract a set of independent variables from  $\xi_{\nu lm}$  's. In general, any  $Q_{\nu lm}$  is related to  $Q_{\nu l-m}$  as

$$Q_{\nu l-m} = (-1)^m Q_{\nu lm}^* F(\nu, l), \quad (57)$$

where

$$F(\nu, l) = \frac{\Gamma(l - \nu i + 1)}{\Gamma(-\nu i)} \frac{\Gamma(\nu i)}{\Gamma(l + \nu i + 1)}. \quad (58)$$

If  $u_\nu$  is real, from Eq.(57),

$$\begin{aligned} u_\nu &= \sum_{lm} \xi_{\nu lm} Q_{\nu lm} \\ &= \sum_{lm} \xi_{\nu lm}^* Q_{\nu lm}^* \\ &= \sum_{lm} (-1)^{-m} \xi_{\nu l-m}^* Q_{\nu lm} F^{-1}(\nu, l), \end{aligned} \quad (59)$$

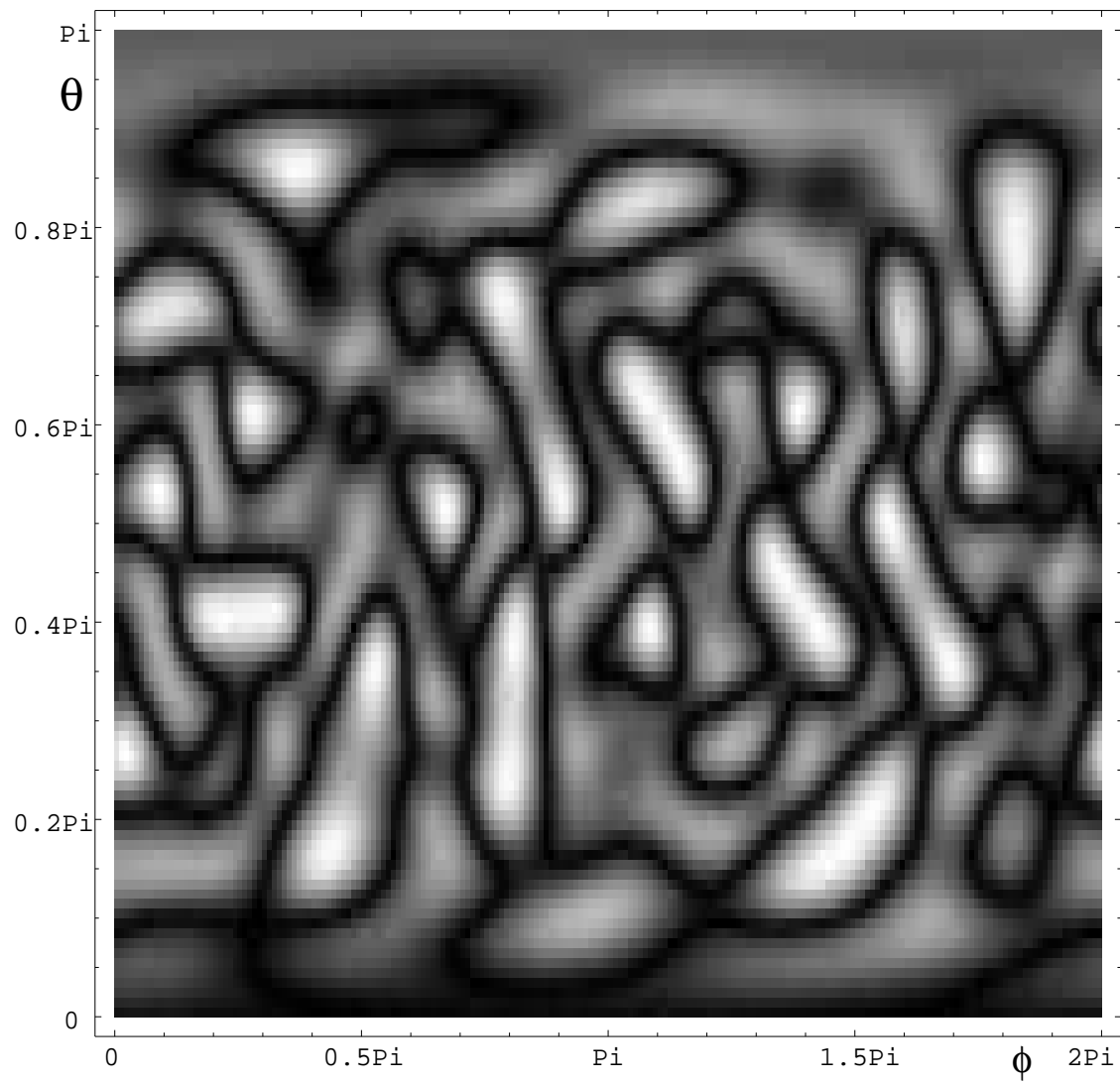


Figure 4: Absolute values of eigenfunction  $u(k = 5.41)$  on sphere  $\chi_o = 1.6$

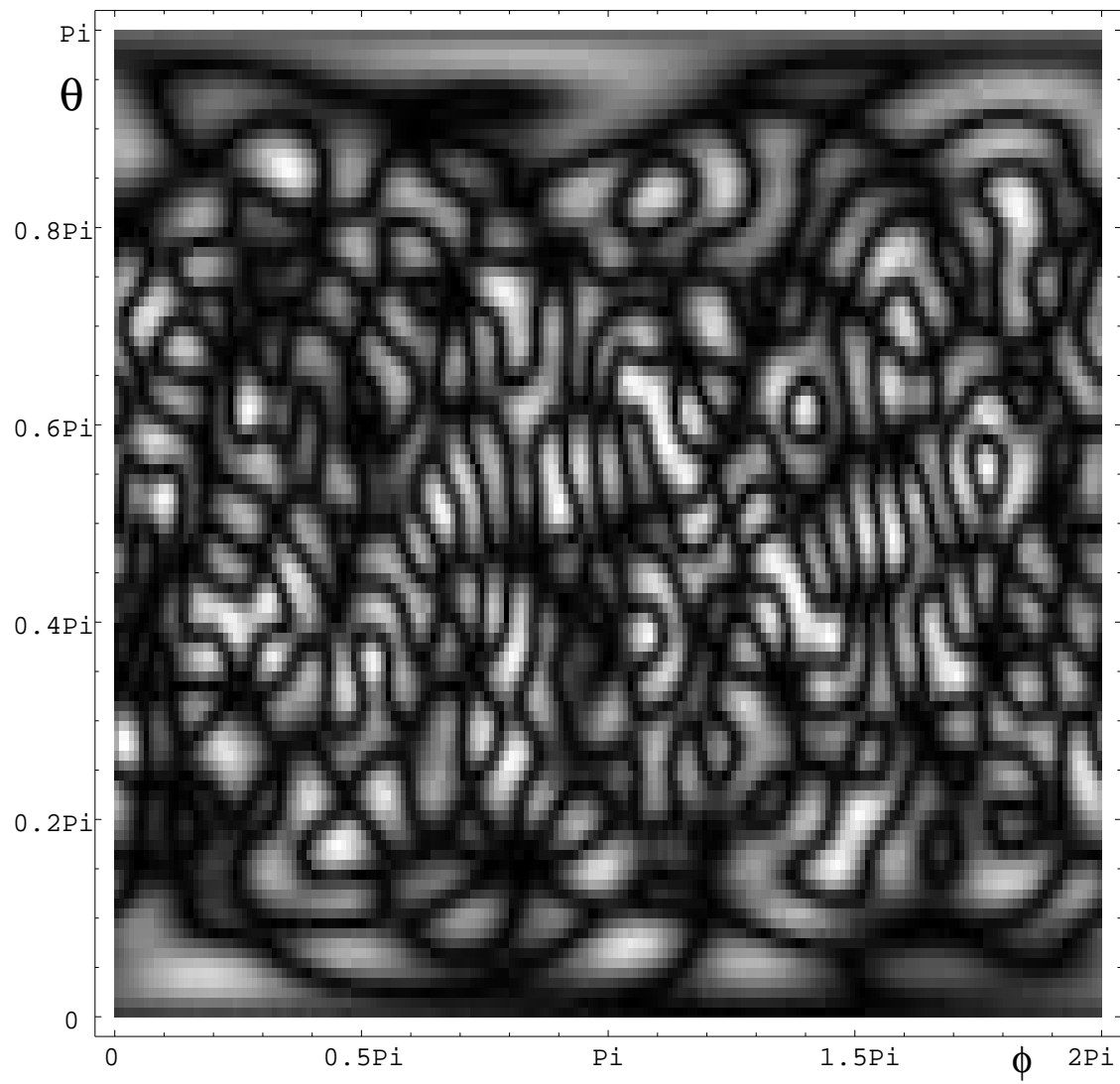


Figure 5: Absolute values of eigenfunction  $u(k = 9.99)$  on sphere  $\chi_o = 1.6$

therefore,

$$\xi_{\nu lm} = (-1)^m \xi_{\nu l-m}^* F^{-1}(\nu, l). \quad (60)$$

Thus  $\xi_{\nu l-m}$  can be written in terms of  $\xi_{\nu lm}$ . To extract a set of independent variables from  $\xi_{\nu lm}$ 's, we rewrite Eq.(59) as follows

$$\begin{aligned} u_\nu &= \sum_{l, m \leq 0} \xi_{\nu lm} Q_{\nu lm} + \sum_{l, m > 0} \xi_{\nu lm}^* Q_{\nu lm}^* \\ &= -\text{Im}(\xi_{\nu 00})\sqrt{2}\text{Im}(Q_{\nu 00}) + \sum_{l > 0} \sqrt{C_{\nu l}}\text{Re}(\xi_{\nu l0})R_{\nu l0} \\ &\quad + \sum_{l > 0, m > 0} \sqrt{2} \left( \text{Re}(\xi_{\nu lm})\sqrt{2}\text{Re}(Q_{\nu lm}) - \text{Im}(\xi_{\nu lm})\sqrt{2}\text{Im}(Q_{\nu lm}) \right), \end{aligned} \quad (61)$$

where

$$R_{\nu l0} = (c_{\nu l})^{-1/2} \left( \text{Re}(Q_{\nu l0}) + \frac{1 - F(\nu, l)}{1 + F(\nu, l)} \text{Im}(Q_{\nu l0})i \right), \quad (62)$$

and

$$c_{\nu l} = 1 - \frac{(1 - F(\nu, l))^2}{2F(\nu, l)} - \left\{ \left( \frac{1 - F(\nu, l)}{1 + F(\nu, l)} \right)^2 + 1 \right\} \text{Im} \left( \frac{\Gamma(l + \nu i + 1)}{\Gamma(\nu i)} \right)^2 \left| \frac{\Gamma(\nu i)}{\Gamma(l + \nu i + 1)} \right|^2. \quad (63)$$

Thus the real eigenfuctions can be written in terms of real independent coefficients  $a_{\nu lm}$  and real-valued  $R_{\nu lm}$ ,

$$u_\nu = \sum_{l, m} a_{\nu lm} R_{\nu lm}, \quad (64)$$

where

$$\begin{aligned} a_{\nu 00} &= -\text{Im}(\xi_{\nu 00}), \quad a_{\nu l0} = \sqrt{C_{\nu l}}\text{Re}(\xi_{\nu l0}), \quad l > 0, \\ a_{\nu lm} &= \sqrt{2}\text{Re}(\xi_{\nu lm}), \quad m > 0, \quad a_{\nu lm} = -\sqrt{2}\text{Im}(\xi_{\nu lm}), \quad m < 0, \end{aligned} \quad (65)$$

and

$$\begin{aligned} R_{\nu 00} &= \text{Im}(Q_{\nu 00}), \\ R_{\nu lm} &= \sqrt{2}\text{Re}(Q_{\nu lm}), \quad m > 0, \quad R_{\nu lm} = \sqrt{2}\text{Im}(Q_{\nu lm}), \quad m < 0. \end{aligned} \quad (66)$$

Now we turn to the statistical properties of the coefficients  $a_{\nu lm}$ . As in [5], we consider the cumulative distribution of following quantities,

$$\frac{|a_{\nu lm} - \bar{a}_\nu|^2}{\sigma_\nu^2} \quad (67)$$

where  $\bar{a}_\nu$  is the mean of  $a_{\nu lm}$ 's and  $\sigma_\nu^2$  is the variance. The cumulative distribution is compared to the cumulative RMT distribution functions which are directly derived from Eq.(48),

$$\begin{aligned} I_\mu(x) &= \int_0^x dx' P_\mu(x') \\ &= \frac{\gamma(\mu/2, \mu x/2)}{\Gamma(\mu/2)}, \end{aligned} \quad (68)$$

where  $\gamma(x, y)$  is the incomplete gamma function. To test the goodness of fit between the computed cumulative distribution function and that predicted by RMT, we use Kolmogorov-Smirnov statistic  $D_N$  which is the least upper bound of all pointwise differences  $|I_N(x) - I(x)|$  [29],

$$D_N \equiv \sup_x |I_N(x) - I(x)|, \quad (69)$$

where  $I_N(x)$  is the empirical cumulative distribution function defined by

$$I_N(x) = \begin{cases} 0, & x < y_1, \\ j/N, & y_j \leq x < y_{j+1}, \\ 1, & y_j \leq x, \end{cases} \quad j = 1, 2, \dots, N-1, \quad (70)$$

where  $y_1 < y_2 < \dots < y_N$  are the computed values of a random sample which consists of  $N$  elements. If  $I_N(x)$  is "close" to  $I(x)$ , the observed  $D_N$  must be so small that it falls within the range of possible fluctuations which depend on the size of the random sample. For the random variable  $D_N$  for any  $z > 0$ , it can be shown that the probability of  $D_N < d$  is given by [30]

$$\lim_{N \rightarrow \infty} P(D_N < d = zN^{-1/2}) = L(z), \quad (71)$$

where

$$L(z) = 1 - 2 \sum_{j=1}^{\infty} (-1)^{j-1} e^{-2j^2 z^2}. \quad (72)$$

From observed maximum difference  $D_N = d$ , we obtain the significant level  $\alpha_D = 1 - P$  which is equal to the probability of  $D_N > d$ . If  $\alpha_D$  is found to be large enough, the hypothesis  $I_N(x) = I(x)$  is verified. The computed cumulative distributions of  $|a_{\nu lm}|^2$  and the GOE( $\mu = 1$ ) prediction  $I_1(x)$  for four examples are plotted in Fig.6, and the maximum difference  $d$  and the significant levels  $\alpha_D$  for



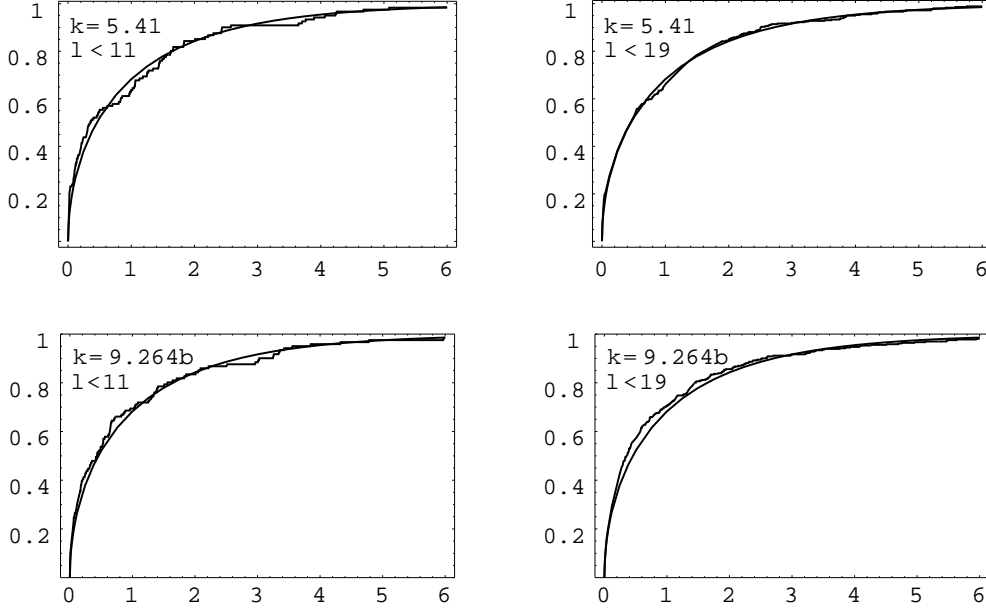


Figure 6: The cumulative distribution of  $|a_{\nu lm} - \bar{a}_{\nu lm}|^2/\sigma^2$  are plotted with the theoretical curve for GOE prediction (full curve). The statistics are based on 121 expansion coefficients for  $l < 11$  and 361 coefficients for  $l < 19$ .

$0 \leq l \leq 10$  and  $0 \leq l \leq 18$  are shown in Table 3. Note that the last digit in  $\alpha_N$  is not guaranteed, since Eq.(71) is an asymptotic formula.

We see from Fig.6 and Table 3 that the agreement with GOE prediction is remarkably good. The gaussian behavior for highly excited states is naturally expected as the semiclassical wavefunctions must reflect the chaotic nature in the corresponding classical systems. However, the gaussian behavior for low-lying modes is not apparent at all. It is possible that the non-gaussianity behavior is rather prominent as these modes have fluctuations on large scale and that reflects the pure quantum mechanical behavior<sup>6</sup>. Nevertheless, our numerical results serve to strengthen the hypothesis that the expansion coefficients behave as Gaussian pseudo-random numbers even for low-lying modes.

<sup>6</sup>The typical scale of angular fluctuation of  $l$  mode is approximately  $\pi/(2l)$  and the typical scale of radial fluctuation of  $k$  mode is approximately given by  $2\pi/k$ .

	$0 \leq l \leq 10$		$0 \leq l \leq 18$	
k	$D_N \times 10^2$	$\alpha_D$	$D_N \times 10^2$	$\alpha_D$
5.41	9.42	23.4%	4.29	51.8%
5.79	3.88	99.3%	4.29	52.1%
6.81	5.95	78.6%	3.47	77.8%
6.89	9.34	24.1%	2.36	98.8%
7.12	7.12	57.2%	2.59	96.8%
7.69	10.23	15.9%	4.84	36.7%
8.30	6.38	70.8%	3.88	65.0%
8.60	5.63	83.8%	2.09	99.7%
8.73	9.46	22.9%	2.78	94.3%
9.26a	7.21	55.6%	3.46	78.1%
9.26b	5.99	77.9%	6.11	13.5%
9.76	7.41	52.0%	4.57	43.8%
9.91	8.90	29.3%	3.23	84.7%
9.99	4.27	98.0%	3.72	70.0%
ave.	7.23	56.3%	3.69	68.8%

Table 3: The Kolmogorov-Smirnov statistics  $D_N$  and the significance levels  $\alpha_D$  for the test of the hypothesis  $I_N(x) \neq I(x)$  and their averages.  $N = 121$  for  $0 \leq l \leq 10$  and  $N = 361$  for  $0 \leq l \leq 18$ . The mode  $k = 9.26$  is degenerated into two modes, which (after orthogonalization) are denoted by  $k = 9.26a$  and  $k = 9.26b$ .

Next we examine the randomness of  $a_{\nu lm}$ 's. Because  $a_{\nu lm}$ 's are actually determined by the Helmholtz equation, it is appropriate to describe  $a_{\nu lm}$ 's as pseudo-random numbers. We apply the run test for testing randomness (see [29]).

Suppose that we have  $n$  observations of the random variable  $X$  and  $m$  observations of the random variable  $Y$ . The combination of those variables into  $m+n$  observations placed in ascending order of magnitude yields

$$\underline{xxx} \underline{yy} \underline{xx} \underline{yyy} \underline{x} \underline{y} \underline{xx} \underline{yy},$$

where  $x$  denotes an observation of  $X$  and  $y$  denotes an observation of  $Y$ . Each underlined group which consists of successive values of  $X$  or  $Y$  is called *run*. The statistics of number of runs are used for testing whether  $X$  and  $Y$  have the same the distribution function. Regardless of the type of the distribution function, the run number  $r$  is known to behave as gaussian random numbers in the limit  $m, n \rightarrow \infty$ .

The run test is also used as a test for randomness. Let  $a_1, a_2, \dots, a_N$  be the observed values of a random variable  $A$ . For simplicity, assume that  $N$  is even. The median divides the observed values into a lower and an upper half. It is represented as  $L$  if it falls below the median, and it is represented as  $U$  if it falls above the median. For instance, a sequence

$$\underline{UUU} \underline{L} \underline{UU} \underline{LL} \underline{U} \underline{U} \underline{L} \underline{UU},$$

has 8 numbers of runs ( $r = 8$ ). The critical region for testing the hypothesis of randomness is of the form  $r < c_1$  or  $r > c_2$  where  $c_1$  and  $c_2$  is readily given by the gaussian distribution function. The significant level  $\alpha_r$  is the probability of  $r > c_1$  or  $r > c_2$ . As the Kolmogorov-Smirnov test,  $\alpha_r$  is given by the observed  $r$ .

The run numbers  $r$  and the significant levels  $\alpha_r$  are shown in Table 4. High significant levels are again observed except for the one at  $k = 8.73$  for  $0 \leq l \leq 18$ . As the corresponding  $r$  is larger than the averaged value, this may be due to the cyclic effect. On the whole, it is concluded that  $a_{\nu lm}$ 's behave as if they are random variables.

	$0 \leq l \leq 10$		$0 \leq l \leq 18$	
k	$r$	$\alpha_r$	$r$	$\alpha_r$
5.41	62	85.5%	185	67.3%
5.79	58	46.5%	174	39.9%
6.81	69	14.4%	196	11.4%
6.89	60	71.5%	168	14.0%
7.12	69	14.4%	184	75.2%
7.69	57	36.1%	191	29.2%
8.30	63	71.5%	177	59.8%
8.60	59	58.3%	184	75.2%
8.73	70	10.0%	201	3.5%
9.26a	56	27.3%	177	59.8%
9.26b	55	20.1%	182	91.6%
9.76	59	58.3%	182	91.6%
9.91	70	10.0%	196	11.4%
9.99	58	46.5%	179	75.2%
ave.	61.8	40.7%	184	50.4%

Table 4: The run numbers  $r$  and the significance levels  $\alpha_r$  for the test of the hypothesis that  $a_{\nu lm}$  's are random variables.  $N = 121$  for  $0 \leq l \leq 10$  and  $N = 361$  for  $0 \leq l \leq 18$ . The mode  $k = 9.26$  is degenerated into two modes, which (after orthogonalization) are denoted by  $k = 9.26a$  and  $k = 9.26b$ .

## 6 Summary

In this paper, we have demonstrated that the DBEM is eminently suitable for computing eigenmodes on CH spaces and we obtain 14 eigenmodes on a CH space called m003(-2,3) which is the second smallest in the known CH manifolds and we have studied the statistical properties of the low-lying eigenmodes.

The low-lying eigenmodes are expanded in terms of eigenmodes on the pseudosphere, and we find that the expansion coefficients behave as if they are gaussian random numbers. Why are they so random even for low-lying modes? It should be pointed out that the randomness of the expansion coefficients for low-lying eigenmodes is not the property of the eigenmodes themselves but rather the property of the images of eigenmodes on the whole universal covering space, since the fluctuation scales for low-lying eigenmodes are comparable to the size of the fundamental domain. We conjecture that the origin of the random behavior of eigenmodes comes from the almost randomly distributed images of a set of points in the universal covering space.

Computation of eigenmodes is essential in simulating the CMB in CH cosmological models. As the DBEM needs only a set of face-to-face identification maps and the discretization of the corresponding fundamental domain, it can be applied to other CH spaces straightforwardly. However, the computation of the modes with small fluctuation scale  $k \gg 1$  is still a difficult task as the number of modes increases as  $N \propto k^3$ .

Nevertheless, the contribution of the modes with small fluctuation to the temperature correlation of CMB can be estimated by assuming that the expansion coefficients for excited states ( $k \gg 1$ ) also behave as gaussian pseudo-random numbers as well as that for low-lying modes. The assumption is numerically confirmed in a two-dimensional CH model [5].

If the observed gaussian pseudo-randomness is found to be the universal behavior in CH spaces for low-lying modes as well as excited modes, the origin of the gaussianity of the CMB fluctuations can be partially explained. This is because the amplitude of the CMB fluctuation is written in terms of:

1. expansion coefficients of the initial fluctuation in terms of eigenmodes on the CH space
2. expansion coefficients of eigenmodes on the CH space that are extended onto the whole pseudosphere in terms of eigenmodes on the pseudosphere.

### Acknowledgments

I would like to thank my advisor Professor Kenji Tomita for his many helpful discussions and continuous encouragement. I would also like to thank Toshiro Matsumoto for his extensive advice on the boundary element methods. I am supported by JSPS Research Fellowships for Young Scientists, and this work is supported partially by Grant-in-Aid for Scientific Research Fund (No.9809834).

### References

- [1] Stevens, D., Scott, D. and Silk, J., Phys. Rev. Lett. **71**, 20 (1993)
- [2] de Oliveira-Costa, A. and Smoot, G.F. and Starobinsky, A.A. ApJ **468**, 457 (1996)
- [3] Levin, J.L., Barrow., J.D., Bunn, E.F. and Silk, J., Phys. Rev. Lett. **79**, 974 (1997)
- [4] Levin, J.L., Scannapieco, E. and Silk, J., astro-ph/9802021
- [5] Aurich, R. and Steiner, F., Physica D **64**, 185 (1993)
- [6] Brebbia, C.A. and Dominguez, J., *Boundary Elements - An introductory Course Second Edition*, Computational Mechanics Publications (1992)
- [7] Tanaka, M., Sladek, V. and Sladek, J., "Regularization techniques applied to boundary element methods", Applied Mechanics Reviews, Vol.47, 457 (1994)
- [8] Beardon, A.E., *The Geometry of Discrete Groups*, Graduate Texts in Mathematics, **91** Springer (1983)

- [9] Löbell, F., Ber, Sächs. Akad. Wiss. Leipzig 83 (1931)
- [10] Seifert, H. and Weber, C., Math. Z. **37**, 237 (1933)
- [11] Best, L.A., Can. J. Math. **23**, No. 3, 451 (1971)
- [12] Thurston, W. P., *The geometry and topology of three manifolds*, Princeton Lecture Notes (1979) (Now available via internet:  
<http://www.msri.org/gt3m/>)
- [13] Benedetti, R. and Petronio, C., *Lectures on Hyperbolic Geometry*, Springer-Verlag (1992)
- [14] Mostow, G.D., Ann. of Math. Studies 78, Princeton (1973)
- [15] Fomenko, A.T. and Kunii, T.L., *Topological Modeling for Visualization*, Springer-Verlag (1997)
- [16] Weeks, J.R., SnapPea: *A computer program for creating and studying hyperbolic 3-manifolds*, available at  
<http://www.geom.umn.edu/software/download/snappea.html>
- [17] Weeks, J.R., PhD thesis, Princeton University (1985)
- [18] Matveev, S.V. and Fomenko, A.T., Russian Math Surveys **43** (1), 3 (1988)
- [19] Hodgson, C. and Weeks, J., Experimental Math., 261 (1994)
- [20] Elstrodt, E., Grunewald, F. and Mennicke, J., Uspekhi Mat.Nauk **38**, No. 1, 119 (1983)
- [21] Tomaschitz, R., Physica D **34**, 42 (1989)
- [22] Telles, J.C.F., International Journal for Numerical Methods in Engineering, **24** 959 (1989)
- [23] Hayami, K. and Brebbia, C.A., *Boundary Elements IX*, Vol.1, 375 (1987)
- [24] Mehta, M.L., *Random Matrices and the Statistical theory of Energy Levels*, Academic Press, New York (1990)

- [25] Bohigas, O., "Random Matrix Theories and Chaotic Dynamics" in Proceedings of the 1989 Les Houches School on Chaos and Quantum Physics, Gian-noni, A., *et al* eds., Elsevier, Amsterdam (1991)
- [26] Haake, F. and Zyczkowski, K., Phys. Rev. A **42** 1013 (1990)
- [27] Brody, T.A., Flores, J., French, J.B., Mello, P.A., Pandey, A. and Wong, S.S.M., Rev. Mod. Phys. **53** 385 (1981)
- [28] Harrison, E.R., Rev. Mod. Phys. **39**, No. 4, 862 (1967)
- [29] Hogg, R.V. and Tanis, E.A., *Probability and Statistical Inference*, Macmillan Publishing Co., Inc., New York (1977)
- [30] Birnbaum, Z.W., *Introduction to Probability and Mathematical Statistics*, Haper & Brothers, New York (1962)